







[View Journal Online](#)
[View Article Online](#)

Synthesis, spectral investigation, biological efficacy, and computational evaluation of the hydroxamic acid chelator and its Zn(II) metal complex with potent anticancer activity

Shubham Sharma ¹, Maridula Thakur ¹, Sohini Sharma ²,
 Shamsheer Singh Kanwar ² and Meena Kumari ^{1,*}

¹ Department of Chemistry, Faculty of Physical Sciences, University of Himachal Pradesh, Shimla-171005, India

² Department of Biotechnology, Faculty of Life Sciences, University of Himachal Pradesh, Shimla-171005, India

* Corresponding author at: Department of Chemistry, Faculty of Physical Sciences, University of Himachal Pradesh, Shimla-171005, India.
 e-mail: drmeenakhandel@gmail.com (M. Kumari).

RESEARCH ARTICLE



doi: 10.5155/eurjchem.15.2.166-177.2527

Received: 22 February 2024

Received in revised form: 14 April 2024

Accepted: 5 May 2024

Published online: 30 June 2024

Printed: 30 June 2024

KEYWORDS

Chelation
 Zinc(II) complex
 Bidentate ligand
 Molecular docking
 Coordination geometry
 3-Methoxybenzohydroxamate

ABSTRACT

The biologically active Zn(II) complex [Zn(HL)₂] (HL = 3-OCH₃C₆H₄-(CO)NHO) has been synthesized by the reaction of ZnSO₄ with potassium 3-methoxybenzohydroxamate (KHL, 3-OCH₃C₆H₄CONHOK) in a 1:2 molar ratio in MeOH solvent medium simply stirring, avoiding drastic conditions and hazardous chemicals. Physicochemical (elemental analysis, molar conductivity) and spectroscopic studies (FTIR, UV-visible, ¹H NMR, and ¹³C NMR) were conducted to characterize the complex. The coordination involving the oxygen atoms of carbonyl and hydroxamic groups (O,O coordination) and the presence of a distorted tetrahedral geometry around the complex have been inferred on the basis of computational studies. Computational investigations indicate that the complex exhibits greater stability in comparison to that of the ligand, and additional calculations were conducted to assess various chemical reactivity parameters. The biological efficacy of the complex has been evaluated through investigations of its antimicrobial, cytotoxic, and anticancer properties, complemented by DNA binding and docking analyzes. The antimicrobial activity of the ligand and the complex against selected bacteria (*S. aureus*, *S. typhi*, *E. coli*, *S. flexneri*) and fungi (*R. solani*, *A. alternata*, and *F. sambucinum*) was also evaluated. The complex was found to be more toxic against the bacterial species *S. typhi* and *E. coli* and showed efficient inhibitory activity against the fungi *F. sambucinum* and *A. alternata*. The results were compared with the standard antibacterial drug tetracycline and the antifungal drug amphotericin B. *In vitro* cytotoxicity assessments were performed using L₂₀B cell lines, which are malignant mouse cells expressing the human poliovirus receptor (CD155), and Rhabdomyosarcoma RD cancer cell lines derived from muscle tissue. The findings revealed decreased cell viability, which is correlated with the increase in the concentrations of the test compounds, demonstrating potent anticancer activity specifically against rhabdomyosarcoma cancer cell lines. Additionally, molecular docking investigations were performed to explore the molecular interactions between the ligand, the complex, and the crystal structure of the *A. alternata allergen* (3V0R), further supporting the efficacy of both the ligand and the complex.

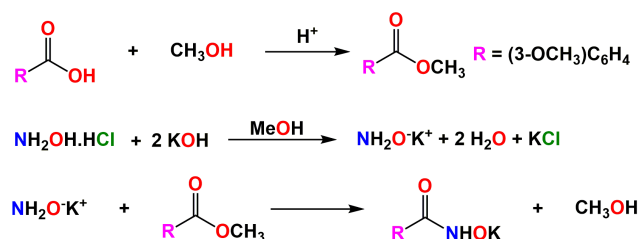
Cite this: *Eur. J. Chem.* 2024, 15(2), 166-177

Journal website: www.eurjchem.com

1. Introduction

Coordination compounds have garnered substantial interest because of their varied structures, which offer versatile applications such as pollutant adsorption and potent heterogeneous photocatalysis for the degradation of organic pollutants and hydrogen production. These functionalities arise from synergistic interactions between metals and functional organic ligands, as well as catalytically active metal sites [1]. Given the *d*¹⁰ configuration of Zn(II), it can adopt various topologies with varying coordination numbers, leading to a wide range of applications. Numerous supramolecular compounds comprising zinc and potassium, which exhibit promising antibacterial activities [2,3], have been successfully

synthesized using the sonochemical method [4-6]. Zinc is a biologically important metal ion and an essential mineral that is of great biological and public health importance [7]. It is a trace metal that is crucial for humans [8], animals [9], plants [10], and microorganisms [11]. Zinc is the exclusive metal present across all enzyme classes and ranks as the second most prevalent transition metal within organisms [10]. Those with zinc deficiency are at increased risk of major depressive disorder (MDD), which can be effectively treated with zinc supplements [12]. Zinc plays a ubiquitous role in human biology and interacts with a wide range of organic ligands [13]. Zinc plays an important role in the processes of DNA replication and transcription within the cell and is a part of several transcription factors.



Scheme 1. Synthesis of the ligand.

Zinc is also well known for its topical treatment of wounds and various dermatological conditions [14-17]. Zinc plays an important role in the immune system and reduces inflammation [18]. The lack of zinc has been associated with pneumonia and bronchitis in children [19]. Ensuring optimal levels of this element is crucial for the functionality of antioxidant enzymes, including zinc-copper superoxide dismutase, which helps prevent damage to purine bases in DNA, thus mitigating the risk of cancer [20-22]. The synthesis of coordination compounds is primarily influenced by factors such as the electronic structure of the metal ion, the availability of coordination sites in the organic ligand, the nature of the bond, or interaction between the metal ion and the ligand, and the coordination number. Zinc is of paramount importance as a trace element for human physiology, contributing to cellular health, and participating in the activity of more than 300 enzymes [23,24]. Different classes of zinc coordination complexes have shown potential in various applications, including radioprotective agents [25], tumor photosensitizers [26], antidiabetic agents [27,28], anticonvulsants [29], anti-inflammatory agents [30], antimicrobial agents [31-38], antioxidants [39], antiproliferative/antitumor agents [40,41] and anti-Alzheimer agents [42].

Hydroxamic acids, a substantial and biologically significant category of organic bioligands, exhibit a wide variety of biological activities and serve as selective inhibitors of numerous enzymes, including matrix metalloproteinases, peroxidases, hydrolases, ureases, lipoxigenases, cyclooxygenases, histone deacetylases, and peptide deformylases [43,44]. Hydroxamic acids have low toxicity [45] and are well known for their chelating behavior toward transition metal ions [46,47], studied both in solution and in the solid state. The hydroxamic acids can be considered chelating ligands that possess at least two electron-rich sites (non-bonding and/or π -electrons) that can coordinate with the metal ion [48,49]. Hydroxamic acids function as bidentate chelators by coordinating through both the carbonyl and hydroxamic oxygen atoms, thereby establishing five-membered rings characterized by either singly deprotonated hydroxamate or doubly deprotonated hydroximato ligands [50]. The affinity between hydroxamic acid and transition metal ions is significant in the X-ray crystal structures of Ni(II)-containing urease [51] or Zn(II)-containing metalloproteins, such as carbonic anhydrase [52]. These compounds have enormous research interest due to their anti-inflammatory, anti-tubercular, antileukemic, antimicrobial [53-55], and tumor inhibiting properties. Furthermore, they serve pivotal functions in the synthesis of various biologically active pharmaceuticals, including antidepressants, antitumor agents, anti-HIV agents, antimalarial agents, antiasthmatic and anti-inflammatory agents [56], along with applications in insecticides, antioxidants and corrosion inhibitors [57]. Given the significant influence of zinc and hydroxamic acids and to investigate their biological effectiveness, the current study endeavors to synthesize the potassium salt of hydroxamic acid along with its Zn(II) complex, and subsequently evaluate their DFT properties, cytotoxicity, molecular docking interactions, and antimicrobial efficacy.

2. Experimental

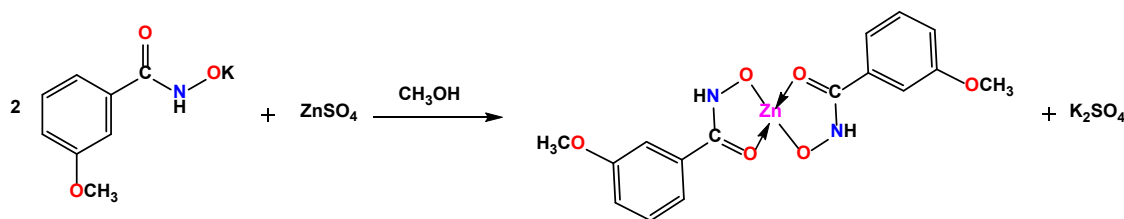
2.1. Materials and instrumentation

The solvents used in the experiment were reagent grade and had been dried and distilled prior to the experiment. Zinc sulfate from Sigma-Aldrich was used without any further processing. Carbon, hydrogen, and nitrogen analyzes using the Carlo-Erba 1106 elemental analyzer. Zinc was estimated by titrating the complex with EDTA and using Erichrome Black-T (EBT) as an indicator [58]. The molar conductance of the complex was evaluated at 30 ± 1 °C utilizing an Elico Conductivity Bridge type CM-82T, a Bench Conductivity / TDS meter with unity cell constant ($K = 1$). Infrared (IR) spectra were obtained using KBr pellets on a PerkinElmer Spectrum RX FTIR spectrophotometer. UV-visible spectra were captured using a Lab India UV-3000 + UV-visible spectrophotometer with standard quartz cells of a path length of 10 mm at a concentration of 5×10^{-5} M at room temperature. ^1H NMR and ^{13}C NMR spectra were recorded on a Bruker Avance Neo 500 MHz NMR spectrometer using DMSO- d_6 as a solvent and TMS as an internal standard. The ligand and complex were optimized using the Orca 4.2.1 program platform [59] and visualized using Chemcraft [60] and Chimera [61]. Molecular docking studies were carried out using the Autodock 4 and Autodock Tools version 1.5.7 [62] version and the results were visualized using Discovery Studio visualizer software [63].

2.2. Synthesis of ligand

The ligand, potassium 3-methoxybenzohydroxamate, was synthesized using the reported method [64,65] (Figure 1). To 5 g of acid (32.9 mmol) was added an excess (up to 10 moles) of methyl alcohol and 1 mL of conc. H_2SO_4 . The reactants are then refluxed on the mantle using a water condenser for 5-7 h. The methyl ester was filtered and dried under vacuum. Separate solutions of $\text{NH}_2\text{OH}\cdot\text{HCl}$ (2.41 g, 34.7 mmol) and KOH (2.92 g, 52.1 mmol) in methanol (10 mL each) were prepared by heating the contents on a water bath. Both solutions were then cooled to 30-40 °C and the solution containing KOH was added with shaking to the solution containing $\text{NH}_2\text{OH}\cdot\text{HCl}$ with simultaneous cooling in an ice bath and allowed to cool in an ice bath for 2-4 h to ensure the complete precipitation of KCl . The mixture was then filtered and to the filtrate was added a methyl ester of the respective acid (2.88 g, 17.3 mmol) with stirring. The mixture is filtered off immediately. The filtrate was allowed to stand for 2-3 days. The solid was filtered off, washed with a little absolute ethyl acetate, and dried in air (Scheme 1).

KHL: Color: Yellow. Yield: 73%. M.p.: 96-98 °C. FT-IR (KBr, ν , cm^{-1}): 3355 (N-H), 1671 (C=O), 1379 (C-N), 935 (N-O), 3025-2810 (Ar. C-H str.). ^1H NMR (500 MHz, DMSO- d_6 , δ , ppm): 3.83 (s, 3H, OCH₃), 6.90-7.82 (m, 4H, Ar-H), 8.00 (s, 1H, N-H). ^{13}C NMR (125 MHz, DMSO- d_6 , δ , ppm): 160.83 (C=O), 55.54 (OCH₃), 101, 104, 108, 114, 119, 122, 129, 130 (Ar-C). Anal. calcd. for $\text{C}_8\text{H}_8\text{KNO}_3$: C, 46.81; H, 3.93; N, 6.82. Found: C, 46.78; H, 3.87; N, 6.79%. UV-Vis (DMSO, λ_{max} , nm, ϵ): 257 (7620).



Scheme 2. Synthesis of Zn(II) hydroxamate complex.

2.3. Synthesis of [Zn(HL)₂]

A solution of zinc sulfate (1 g, 6.21 mmol) in methanol (10 mL) was added to a solution of potassium 3-methoxybenzohydroxamate (KHL) (2.062 g, 12.42 mmol) in 15 mL of methanol and the reaction mixture was stirred for 0.5 h. The yellow complex was precipitated, filtered, and recrystallized from a 1:1 mixture of methanol and diethyl ether (Scheme 2).

[Zn(HL)₂]: Color: Yellow. Yield: 87%. Dec. Temp.: 181-184 °C. FT-IR (KBr, ν , cm^{-1}): 3365 (N-H), 1640 (C=O), 1377 (C-N), 955 (N-O), 2965-2790 (Ar. str.), 485 (Zn-O). ¹H NMR (500 MHz, DMSO-*d*₆, δ , ppm): 7.55 (t, $J = 7.4$ Hz, 1H, NH), 7.50 (s, 1H, NH), 7.48-7.42 (m, 2H, Ar-H), 7.41-7.29 (m, 4H, Ar-H), 7.05 (td, $J = 9.4, 2.7$ Hz, 2H, Ar-H), 3.85-3.76 (s, 6H, OCH₃). ¹³C NMR (125 MHz, DMSO-*d*₆, δ , ppm): 165.97 (C=O), 55.25 (OCH₃), 110, 113, 116, 118, 119, 121, 128, 129, 130 (Ar-C). Anal. calcd. for C₁₆H₁₆O₆N₂Zn: C, 48.32; H, 4.06; N, 7.04. Found: C, 48.31; H, 3.99; N, 7.01%. UV-Vis (DMSO, λ_{max} , nm, (ϵ)): 298 (5940). Λ_{m} (DMSO, 1×10^{-3} M, 30 °C, S.cm²/mol): 1.085.

2.4. Computational assessment using DFT

The structures for computational studies were prepared in Chemcraft [60] and the reported compounds were optimized by Orca 4.2.1 program platform [59] and analyzed by Chimera 1.17.3 [61]. A very useful method for exchange correlation functional, *i.e.*, B3LYP [66], is applied with the Def2-SVP basis set [67]. Energy-optimized structures and various chemical reactivity parameters for the ligand and complex were calculated.

2.5. Antimicrobial activity assay by two-fold serial dilution method

In vitro antibacterial and antifungal activities of the ligand and Zn(II) hydroxamate by the minimum inhibitory concentration (MIC) method [68] are tested in a 96-well microtitre plate (tissue culture grade) by the two-fold serial dilution method [68] using Resazurin, an oxidation reduction colorimetric indicator dye to determine drug resistance and minimal inhibitory concentration against different microorganisms [69]. The dye turns pink from its blue oxidized state upon reduction by viable cells, which indicates the growth of bacteria and fungi. The lowest concentration of the complex that prevented this color change was considered MIC according to the Clinical and Laboratory Standards Institute (CLSI M07-A9) [70]. A stock solution of ligand and complex were prepared in DMSO (250 $\mu\text{g}/\text{mL}$). A set of 12 wells was utilized for the minimum inhibitory concentration assay, with the final two wells serving as controls. Each of the ten wells received 50 μL of Muller-Hinton broth, except for the first well, which contained 100 μL of broth and 250 $\mu\text{g}/\text{mL}$ of the test complex. From the first well containing the test complex, 50 μL of broth was transferred to the second well and the contents were thoroughly mixed. This serial dilution process was repeated, resulting in a range of two-fold serial dilutions (250-0.90 $\mu\text{g}/\text{mL}$). Resazurin, prepared as a 0.02% weight/volume solution in distilled water and sterilized by filtration, was added to each well. Subsequently, 10

μL of microbial culture was inoculated into each well and the contents were thoroughly mixed by ten clockwise and anticlockwise rotations. Plates were then incubated at 35 °C for 24 hours for bacteria and 28 °C for 72 hours for fungi. To assess the solvent's role in biological screening, studies were also conducted using DMSO which showed no activity. The standard antibacterial drug tetracycline and the antifungal drug amphotericin B were used for comparison. All experiments were performed in triplicate.

2.6. Cytotoxicity studies

Determination of the toxicity of the ligand and the complex was performed via the 3-(4,5-dimethylthiazol-2-yl)-2,5-diphenyltetrazolium bromide (MTT) assay [71] in the concentration range of 5 to 35 $\mu\text{g}/\text{mL}$ of L₂₀B cell lines, a malignant mouse cell line expressing the Human Polio Virus receptor (CD155) and rhabdomyosarcoma RD cancer cell lines isolated from muscle tissue [72]. Rhabdomyosarcoma is a form of cancer that develops from mesenchymal cells of skeletal muscle. Briefly, cells were obtained from the Central Research Institute, Kasauli, India, and the National Center for Cell Science, Pune India. Cell lines were maintained in Dulbecco's Modified Eagle's Medium (Himedia, Mumbai) supplemented with 10% fetal bovine serum, 100 $\mu\text{g}/\text{mL}$ penicillin, and 100 $\mu\text{g}/\text{mL}$ streptomycin. The cell lines were cultured in a humidified atmosphere (95%) with 4% CO₂ at 37 °C. The cells were aseptically seeded in a 96-well plate at a concentration of 1.2×10^4 cells/mL DMEM supplemented with 10% fetal bovine serum (FBS) and allowed to grow overnight. After 24 h, 20 μL solution of each compound with specific concentrations (5, 15, 25, and 35 $\mu\text{g}/\text{mL}$) was then added per well, followed by overnight incubation at 37 °C. Subsequently, the medium was removed and 100 μL fresh medium containing 20 μL of MTT was added, followed by incubation in a CO₂ incubator at 37 °C for 4 hours. After incubation of cells for an additional 4 h with MTT-containing medium, it was withdrawn and 100 μL of DMSO was added to each well to extract the precipitated intracellular purple formazan crystals and shaken for 15 min. The absorbance of the plate was recorded using an automated plate reader (Thermo Fisher Scientific, China) at 570 nm (Equation 1). The control cell measurement values were 0.134 and 0.672 for L₂₀B and RD cells, respectively, to calculate the % cell viability. The experiments were performed in triplicate.

$$\% \text{ Cell viability} = \frac{\text{Absorbance (sample)}}{\text{Absorbance (control)}} \times 100 \quad (1)$$

2.7. Molecular docking and DNA binding studies

The protein structure of *A. alternata* allergen Alt a 1, with PDB ID: 3VOR, and the crystal structure of double-stranded DNA (PDB ID 1AIO) featuring specific DNA sequences (5'-D(CCTCTGGTCTCC)-3', 5'-D(GGAGACCAGAGG)-3') for the DNA binding studies was obtained from the RCSB (Royal Col Laboratory for Structural Bioinformatics) database at www.rcsb.org [73]. The PDB structures of the ligand and its complex were generated using Pymol [74]. Then the pdbqt files

(structure files with added Kolmann charges) were generated for the ligands and their complexes [75]. The protein's binding site was located using grid dimensions, and the ligand and synthesized complex were docked into the binding site using AutoDock4 and AutoDock tools [62]. To discern distinctive conformations, a root mean squared tolerance (RMS) of 2.0 Å was applied. Ten cluster ranks of ligand and complex interactions were executed across diverse conformations to assess the optimal energy states. The data obtained were analyzed using Discovery Studio (DS) visualizer software [63]. Results encompassing the lowest docking binding energy, average binding energy, final intermolecular energy, inhibition constants, total internal energy, and other pertinent parameters were then computed.

3. Result and discussion

3.1. Synthesis

The complex $[Zn(HL)_2]$ has been synthesized in quantitative yields by the reaction of $ZnSO_4$ with potassium salt of 3-methoxybenzohydroxamate in a 1:2 ratio in methanol, according to Scheme 2. The complex is yellow in color and soluble in DMSO, chloroform, sparingly in dichloromethane, etc. The conductance value in DMSO was low, that is, 1.085 S.cm²/mol, suggesting that no anions are present outside the coordination sphere, confirming its nonelectrolytic nature [76]. The complex is soluble in organic solvents such as DMSO, chloroform, and dichloromethane, although to a lesser extent in the latter. Computational, physicochemical, and spectral investigations confirmed the presence of a four-coordinate distorted tetrahedral geometry around zinc. Furthermore, DFT analysis and low molar conductance values (indicating the nonelectrolytic character) provide additional support for the stability and geometry of the complex. Moreover, the absence of significant color alteration upon dissolution serves as further evidence of its stability. Spectral studies were conducted using both solid-phase (IR spectra) and solution-phase (¹H NMR, ¹³C NMR spectra) samples, and the bands observed with almost similar values indicate that the structure of the complex remains unchanged in both phases.

Comparison of FT-IR spectra of the synthesized complex with a free ligand showed its formation. The bands at 3355 and 1379 cm⁻¹ in the free ligand, assigned to $\nu(NH)$ and $\nu(CN)$ modes, respectively, did not undergo any change in the respective complex. This suggests that the NH group is retained, and coordination through the nitrogen atom is excluded. The absorption band at 1671 cm⁻¹ due to $\nu(C=O)$ mode appears at a lower frequency at 1638 cm⁻¹ in the complex. In addition, the sharp band appearing at 935 cm⁻¹ in the free ligand has been observed at 955 cm⁻¹ in the complex, which may be attributed to the $\nu(NO)$ mode. A shift in $\nu(C=O)$ mode to a lower wavenumber and that of $\nu(NO)$ mode to a higher region suggests the bonding of carbonyl and hydroxylamine oxygen atoms, establishing the bidentate nature of the ligand. The band appearing at 485 cm⁻¹ may be ascribed to the $\nu(M-O)$ bond ($M=Zn$) in the complex [77].

At room temperature, KHL and its complex were prepared with a concentration of 5.0×10^{-5} M in DMSO. The ligand and the complex exhibit sharp bands at 257 nm ($\epsilon = 7620$ M⁻¹.cm⁻¹) and 298 nm ($\epsilon = 5940$ M⁻¹.cm⁻¹) in the UV region, which may be attributed to the intraligand $\pi \rightarrow \pi^*$ or $n \rightarrow \pi^*$ transitions. The complex exhibits a minor red shift in wavelength signaling complexation. However, no notable absorption was detected in the visible region of the Zn(II) complex, which could be attributable to the complete occupancy of the *d*-orbitals.

The ¹H NMR spectrum of the hydroxamate ligand KHL was compared to the complex. The free ligand exhibits signals due to its aromatic protons at δ 6.90-7.82, NH at δ 8.00, and OCH₃ at δ 3.83 ppm. Whereas, the complex shows a signal at δ 7.05-7.55,

7.50, and 3.83 ppm due to its aromatic protons, NH and OCH₃, respectively. The complex showed a singlet at δ 7.50 ppm due to NH and another singlet at δ 3.85-3.76 ppm attributed to 6 OCH₃ protons. Two multiplets of 2 Ar-H and 4 Ar-H were observed at δ 7.48-7.42 and 7.41-7.29 ppm, respectively. Furthermore, a triplet of doublet (td) was observed at δ 7.05 ppm due to 2 Ar-H of the aromatic ligand. A triplet at δ 7.55 ppm was observed due to the N-H coupling with a coupling constant of 7.4 Hz. The slight upfield observed in the signals of aromatic protons in the complex supports its formation.

The ¹³C NMR spectra of KHL showed signals between δ 101.17 and 130.22 ppm due to aryl carbons. Furthermore, the peak at δ 160.83 ppm was assigned to the carbon atom signal of the carbon-oxygen double bonds (C = O) in *keto* form. The carbon of the methoxy group was observed at δ 55.54 ppm for KHL. On the other hand, the complex showed signals between δ 110.91 and 130.90 ppm for aromatic carbons. The C=O and methoxy peaks were observed at δ 165.97 and 55.25 ppm for the complex, respectively. The hydroxamate ligand is known to exist in two tautomeric forms, *keto* and *enol*. However, analysis of the ¹³C-NMR data for both the ligand and complexes revealed the predominance of the *keto* form in DMSO solution, as evidenced by the presence of sharp signals corresponding to the C=O group. This confirms the O,O coordination to the metal ion. Typically, the polar solvent dimethylsulphoxide facilitates a reversible proton transfer process, where tautomeric conversion occurs from the OH to the NH form [78]. However, in this case, no such change was observed.

3.2. Computational analysis

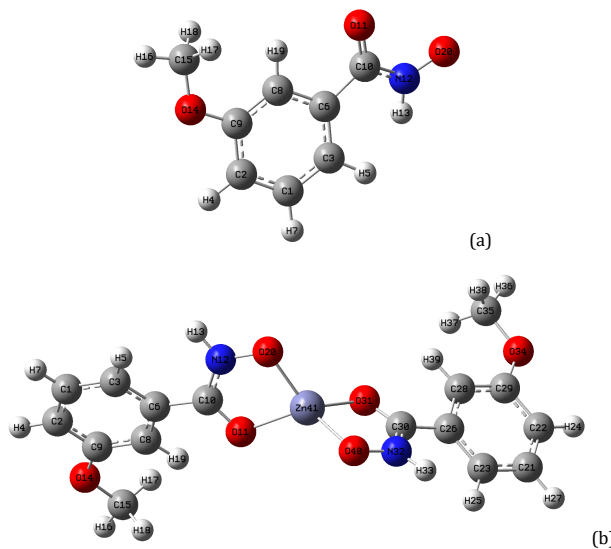
The geometry optimization was performed utilizing ORCA 4.2.1 Program platform [59] using the DFT method [79] to understand the electronic structure of a ligand and its complex with the B3LYP/Def2-SVP basic set [66,67]. The optimized geometry of the complex was determined to be distorted tetrahedral on the basis of calculations. The geometrical and structural parameters calculated are provided in Table 1. Figures 1a and 1b depict the energy-optimized structures of the ligand and complex, respectively.

3.2.1. Structural analysis

The optimization of the Zn(II) complex revealed a distorted tetrahedral configuration around the zinc metal ion. The ligand KHL engages in bidentate coordination with the metal ion, utilizing both the carbonyl oxygen and oxygen from the hydroxylamine group. Analysis of the computed molecular structure of $[Zn(HL)_2]$ indicates a slight elongation of C=O bond lengths (C30-O31 = 1.271 Å, C10-O11 = 1.272 Å) by approximately +0.022 and +0.023 Å, respectively, compared to the free ligand, suggesting a minor reduction in double bond character and the bonding via the carbonyl oxygen to the central metal ion. This is further supported by the presence of C=O signals in the ¹³C NMR spectrum of the complex. The NO (N12-O20 = 1.344 Å, N32-O40 = 1.343 Å) bond lengths exhibit a slight increase of approximately +0.048 and +0.049 Å compared to the free ligand. Conversely, the CN (C30-N32 = 1.331 Å, C10-N12 = 1.331 Å) bond lengths are slightly reduced by approximately -0.026 Å relative to the free ligand (C10-N12 = 1.357 Å). The Zn-O bond distances (Zn41-O20 = 1.959 Å and Zn41-O40 = 1.9577 Å) involving hydroxamic oxygen are shorter than the Zn-O bond distances (Zn41-O11 = 2.026 Å and Zn41-O31 = 2.027 Å) involving carbonyl oxygen. Bond angles around zinc range from 83.65 to 129.15° in the complex. The observed alterations in bond lengths (CO, CN, and NO) and various bond angles indicate bonding through carbonyl and hydroxamic oxygen to the metal ion. Minor deviations in the coordination environment of the zinc metal ion from an ideal tetrahedral arrangement are ascribed to the structural limitations imposed

Table 1. Calculated bond lengths (Å) and bond angles (°) for the ligand and the complex from DFT calculations.

Bond lengths		Bond angles	
HL - B3LYP/DEF2-SVP			
N12-H13	1.028	C10-N12-O20	127.69
N12-O20	1.295	C10-N12-O11	125.28
C10-O11	1.249	C15-O14-C9	118.23
C10-N12	1.357	C6-C10-N12	113.70
C9-O14	1.375	O20-N12-H13	116.94
C15-O14	1.404	C6-C10-O11	120.92
C6-C10	1.503	C2-C9-O14	115.79
C2-C9	1.406		
C8-C9	1.395		
[Zn(HL)₂] - B3LYP/DEF2-SVP			
Zn41-O40	1.957	O40-Zn41-O31	83.65
Zn41-O31	2.027	O11-Zn41-O20	83.59
Zn41-O20	1.959	O40-Zn41-O11	123.17
Zn41-O11	2.026	O31-Zn41-O20	123.83
N32-O40	1.343	O31-Zn41-O11	118.21
N12-O20	1.344	O20-Zn41-O40	129.15
C30-O31	1.271	Zn41-O20-N12	106.85
C10-O11	1.272	Zn41-O11-C10	108.68
C29-O34	1.355	O11-C10-N12	119.12
C9-O14	1.355	C9-O14-C15	119.28
C15-O14	1.412	Zn41-O40-N32	106.88
C35-O34	1.412	Zn41-O31-C30	108.55
C30-N32	1.331	O40-N32-C30	121.70
C10-N12	1.331	N32-C30-O31	119.19
		C29-O34-C35	119.32
		C26-C30-O31	121.53
		C6-C10-O11	121.39
		C6-C10-N12	119.46
		C29-O34-C35	119.32

**Figure 1.** Energy optimized geometry of ligand (a) and Zn complex (b).

by the presence of the hydroxamate ligand. The presence of two shorter ZnO bond lengths (Zn41-O20 = 1.959 Å, Zn41-O40 = 1.957 Å) corresponds to smaller bond angles (O20-Zn41-O11 = 83.59°, O31-Zn41-O40 = 83.65°), while the two longer bond lengths (Zn41-O11 = 2.026 Å, Zn41-O31 = 2.027 Å) are associated with larger bond angles (O20-Zn41-O40 = 129.15°, O20-Zn41-O31 = 123.83°, O11-Zn41-O40 = 123.17°, O11-Zn41-O31 = 118.21°) than those expected in a regular tetrahedral geometry, confirming the attainment of a distorted tetrahedral geometry in the complex.

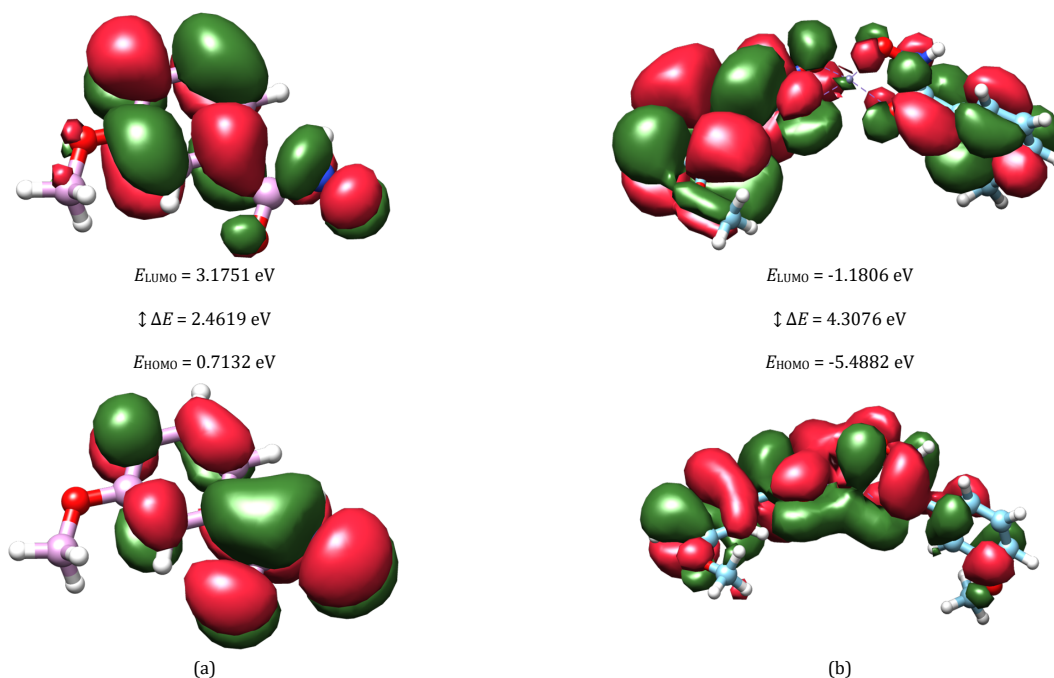
3.2.2. Frontier molecular orbitals

Frontier molecular orbital analyses reveal the reactive site within a conjugate system and offer insight into the complexation process. Molecular energies of E_{HOMO} (Highest Occupied Molecular Orbital) and E_{LUMO} (Lowest Unoccupied Molecular Orbital) were used to compute chemical reactivity descriptors,

including chemical potential, chemical hardness, and electrophilicity. Electronegativity, global hardness, chemical potential, global softness, and global electrophilicity index were additionally determined to characterize the chemical reactivity of the compound and particular reactive sites within the molecular system. The HOMO and LUMO energy levels for the ligand were 0.7132 and 3.1751 eV, respectively, with a HOMO-LUMO energy gap (ΔE) of 2.4619 eV. For complex, the HOMO and LUMO energy levels were -5.4882 and -1.1806 eV, respectively, with a HOMO-LUMO band gap (ΔE) of 4.3076 eV. The HOMO-LUMO energy gap representation for the ligand and the respective complex can be seen in Figures 2a and 2b. Visualization of the highest occupied molecular orbitals (HOMOs) of the complex reveals their delocalization, predominantly residing on the orbitals associated with Zn(II). On the contrary, the lowest unoccupied molecular orbitals exhibit comparatively less localization, spreading across the orbitals of the entire ligand fragment within the complex.

Table 2. Representation of various quantum chemical parameters from DFT calculations.

Quantum chemical parameters	Ligand	Complex
Final single point energy (Hartree, E_h)	-589.29	-2957.74
E_{HOMO} (eV)	0.7132	-5.4882
E_{LUMO} (eV)	3.1751	-1.1806
ΔE (eV)	2.4619	4.3076
Dipole moment (D)	10.01	2.16
χ (eV)	-1.944	3.334
η (eV)	1.231	2.1538
σ (eV ⁻¹)	0.812	0.464
μ (eV)	1.944	-3.334
S (eV)	0.406	0.2321
ω (eV)	1.534	2.581

**Figure 2.** HOMO-LUMO representation of ligand (a) and Zn(II) complex.

A closer examination of the electron cloud of the HOMO orbital of the ligand suggests a sharp localization of the electron density on the hydroxamic group, indicative of favorable nucleophilic sites [75]. The negative frontier HOMO-LUMO structure orbital energies for the zinc hydroxamate complex demonstrate the molecular chemical stability [80]. The energy difference between the HOMO and the LUMO ascertains the charge-transfer interaction. Global hardness and global softness were also predicted. The larger value of $\Delta E = E_{LUMO} - E_{HOMO}$ for the complex than the ligand confirms that the complex is more stable. Furthermore, the electrophilicity index (ω), exhibiting a higher positive value for the complex compared to the ligand ($2.581 > 1.534$ eV), quantifies the system's propensity to accept an electron from the environment. This observation confirms the enhanced stability of the complex relative to that of the unbound ligand.

3.2.3. Chemical reactivity descriptors

Ionization potential (IP), electron affinity (EA), electronegativity (χ), global hardness (η), chemical potential (μ), global softness (S), and global electrophilicity index (ω) play a vital role in explaining the chemical reactivity and stability of a molecular system. The chemical hardness, denoted by $\eta = (E_{LUMO} - E_{HOMO})/2$, indicates the stability and reactivity of any chemical system. Electronegativity delineates an atom's capacity within a molecule to draw electrons toward itself, as expressed by $\chi = -(E_{HOMO} + E_{LUMO})/2$. Chemical potential is negative of electronegativity and is represented by $\mu = (E_{HOMO} +$

$E_{LUMO})/2$. The electrophilic index, which is calculated using $\omega = \mu^2/2\eta$, is an indicator of the capacity of a system to accept electrons. The global softness can be determined using the expression $S = 1/2\eta$. The disparity between the energy levels of the highest occupied molecular orbital and the lowest unoccupied molecular orbital offers an understanding of charge transfer interactions. Furthermore, the chemical potential (μ) provides insight into the charge transfer within the ground state of any compound. Moreover, electrophilicity (ω) serves as a thermodynamic parameter that quantifies energy alterations when a chemical system becomes saturated upon the addition of electrons, assigning a greater positive value to the complex (2.581 eV) than the ligand (1.534 eV) quantifies the system's tendency to accept an electron from the surroundings ascertaining the complex to be more stable. Table 2 represents the quantum chemical parameters calculated for the ligand and the complex.

3.3. Antimicrobial activity

The *in vitro* antimicrobial efficacy of the ligand and complex was assessed against specific strains of Gram-positive bacteria *S. aureus* and Gram-negative bacteria *S. typhi*, *E. coli*, and *S. flexneri*, as well as pathogenic fungi *R. solani*, *A. alternata*, and *F. sambucinum* at varying concentrations in DMSO employing the standard MIC method recommended by the National Committee for Clinical Laboratory Standards (NCCLS) [70]. The commercial antibiotics tetracycline and amphotericin B were used as reference standards for comparative analysis.

Table 3. Antibacterial activity data by the MIC method in $\mu\text{g/mL}$ (\pm standard deviation).

Compound	<i>S. aureus</i>	<i>S. typhi</i>	<i>E. coli</i>	<i>S. flexneri</i>
KHL	125 \pm 0.30	62.5 \pm 0.02	15.63 \pm 0.20	31.25 \pm 0.40
Complex	31.25 \pm 0.30	31.25 \pm 0.04	7.80 \pm 0.02	15.63 \pm 0.03
Tetracycline	3.90	15.63	15.63	15.63

Table 4. Antifungal activity data by the MIC method in $\mu\text{g/mL}$ (\pm standard deviation).

Compound	<i>R. Solani</i>	<i>A. alternata</i>	<i>F. sambucinum</i>
KHL	125 \pm 0.01	31.25 \pm 0.45	31.25 \pm 0.02
Complex	15.63 \pm 0.04	7.80 \pm 0.05	15.63 \pm 0.03
Amphotericin B	1.95	0.25-1.00	0.5-1.00

Table 5. *In vitro* cytotoxicity data by the MTT assay of L₂₀B cell lines (\pm standard deviation).

Concentration ($\mu\text{g/mL}$)	% Cell viability of L ₂₀ B cells		% Cell viability of RD cells	
	Ligand	Complex	Ligand	Complex
5	29.67 \pm 0.02	19.15 \pm 0.50	12.5 \pm 0.30	7.8 \pm 0.20
15	17.21 \pm 0.30	8.73 \pm 0.03	8.45 \pm 0.50	5.15 \pm 0.40
25	9.21 \pm 0.04	3.21 \pm 0.20	5.9 \pm 0.10	3.4 \pm 0.03
35	3.57 \pm 0.10	0.99 \pm 0.01	3.2 \pm 0.04	1.9 \pm 0.04

The free ligand and the complex were screened *in vitro* for their antibacterial activity against different bacteria such as *S. aureus*, *S. typhi*, *E. coli*, and *S. flexneri* (Table 3). The results were compared with the standard drug tetracycline. KHL inhibited the growth of Gram-positive *S. aureus* and Gram-negative *S. typhi* at 125 and 62.5 $\mu\text{g/mL}$, respectively. *E. coli* and *S. flexneri* were inhibited at 15.63 and 31.25 $\mu\text{g/mL}$, respectively. The complex showed promising activity against the selected microbes in the MIC range of 7.80-31.25 $\mu\text{g/mL}$. The complex was found to be more toxic against *E. coli* and with a MIC value of 7.80 $\mu\text{g/mL}$.

The ligand and complex were assayed against the selected fungi, i.e., *R. solani*, *A. alternata*, and *F. sambucinum*. The results were compared with the standard antibiotic amphotericin B (Table 4). The complexes showed enhanced activity over the ligands. The free KHL showed an inhibitory effect against *R. solani*, *A. alternata*, and *F. sambucinum* at a MIC of 125, 31.25, and 31.25 $\mu\text{g/mL}$, respectively. The complex inhibited *R. solani* and *A. alternata* at MIC 15.63 and 7.80 $\mu\text{g/mL}$, respectively. The hydroxamate complex showed enhanced activity against *A. alternata* at 7.80 $\mu\text{g/mL}$, being quite effective against it.

The ability of metal complexes to inhibit microbial growth is mainly due to their bacteriostatic effect. The potency of these complexes depends on several factors such as the metal's nature [81], the ligand's ability to easily dissociate, and the nuclearity of the complexes. The interaction of these complexes with the membrane alters its fluidity, potentially targeting the cytoplasmic membrane [82]. The increased antimicrobial activity observed in complexes, in contrast to the free ligand, can be rationalized by chelation theory [83], in which complexation inhibits cell respiration and reduces the polarity of the central metal ion. This partial sharing of the positive charge with the ligand's donor atoms enhances electron delocalization across the entire chelate ring [84], thus amplifying the complex's lipophilicity and hydrophobic properties. This, in turn, favors facilitated perforation through the lipid bilayer membrane [85]. The observed antimicrobial activity of the complex can be attributed to the biological significance associated with the Zn(II) ion and the bioactive hydroxamate ligand.

3.4. Cytotoxicity

In vitro cytotoxicity of the ligand and its Zn(II) hydroxamate complex was carried out on the L₂₀B cell line, a malignant mouse cell line expressing the human poliovirus receptor (CD155). Anticancer activity was evaluated using RD Rhabdomyosarcoma cancer cell lines derived from muscle tissue. Cells were exposed to different concentrations of ligand and complex (5, 15, 25, and 35 $\mu\text{g/mL}$) and then cultured for 24 hours. Cell viability was evaluated using the MTT assay, which quantifies

mitochondrial dehydrogenase activity. The findings demonstrated that higher concentrations of both the ligand and the complex were correlated with a reduction in cancer cell count, confirming their cytotoxic effects. Table 5 represents the cytotoxicity data plot, cell viability percentage of the ligand and complex, and the viability variation of the complex with cell lines. Cell viability of 1% was observed at a concentration of 35 $\mu\text{g/mL}$ for the complex against L₂₀B cell lines. The complex exhibited an increased anticancer efficacy against rhabdomyosarcoma cancer cell lines, demonstrating a cell viability of 1.9% at 35 $\mu\text{g/mL}$, indicating its effectiveness. Furthermore, cell viability decreased significantly with increasing concentrations of the complexes. In particular, the complex demonstrated superior efficacy compared to the ligand against the chosen cell lines (L₂₀B and RD), showing high cell inhibition even at lower concentrations.

3.5. DNA binding studies (1A10)

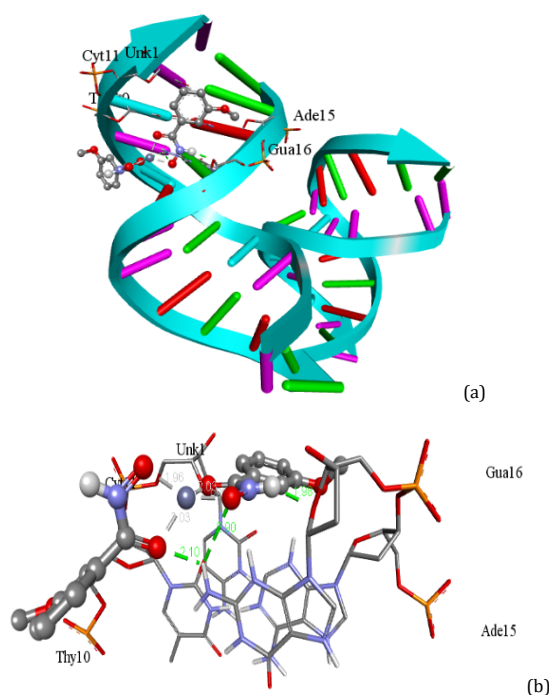
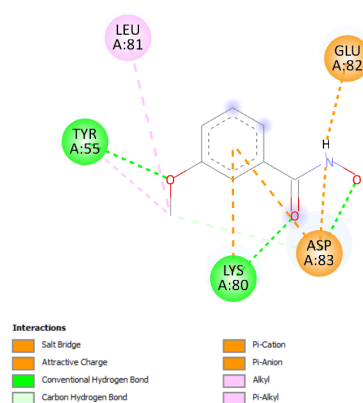
To fortify the anticancer potential of the zinc complex, DNA binding studies were conducted by molecular docking, using the crystal structure of double-stranded DNA (PDB ID 1A10) featuring specific DNA sequences (5'-D(CCTCTGGTCTCC)-3', 5'-D(GGAGACCAGAGG)-3'). Evaluation of the complex's binding affinity with the DNA structure is provided in the accompanying table. The compound exhibited considerable binding efficacy with DNA. Specifically, it demonstrated a free binding energy to the DNA strand of -7.90 kcal/mol, accompanied by an inhibitory constant of 1.62 μM (Table 6). The interaction between DNA and the complex primarily involves conventional hydrogen bonding between the complex and the nucleotide residues. In particular, it formed three conventional hydrogen bonding interactions with ADE-15 and GUA-16 residues (Figures 3a and 3b). Furthermore, in addition to hydrogen bonding, the complex engaged with CYT-11, UNK-1, and THY-10 residues through alternative mechanisms such as metal acceptor interactions and π - π T shaped interactions. The increasingly negative value of the binding energy confirms a robust interaction between the complex and DNA, affirming its potential effectiveness in DNA binding.

3.6. Molecular docking studies

Molecular docking is a key aspect of drug design, facilitating the understanding of interactions between proteins and ligands. By analyzing the mechanistic pathway of docking, it determines the probable binding site and the mode of binding [86], which is usually noncovalent. In this context, the molecular docking of the free ligand and its Zn(II) complex with the crystal structure of *A. alternata* allergen alt a 1 protein (PDB ID = 3V0R) was performed to predict the binding affinity.

Table 6. DNA binding score of the complex with 1A10 DNA strand.

Thermodynamic parameters (Kcal/mol)	Complex (1A10)
Free energy of binding	-7.90
Mean binding energy	-7.79
Final intermolecular energy	-9.00
Electrostatic energy	-0.23
Vdw + H bond + desolve energy	-8.77
Final total internal energy	-0.38
Free energy (A)	-1371.41
Torsional free energy	+1.10
Internal energy (U)	-7.18
Unbound system energy	-0.38
Inhibition constant (μM) (T = 298.15 K)	1.62
Entropy (S) (Kcal/mol/K)	4.58
Partition function (Q)	10.12
Type and number of binding formed	3 Hydrogen bonds (1.90, 2.10 and 2.90 Å)

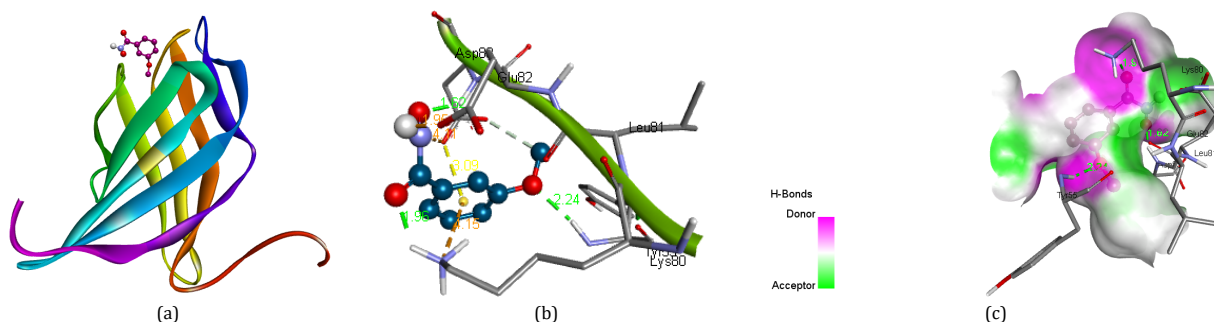
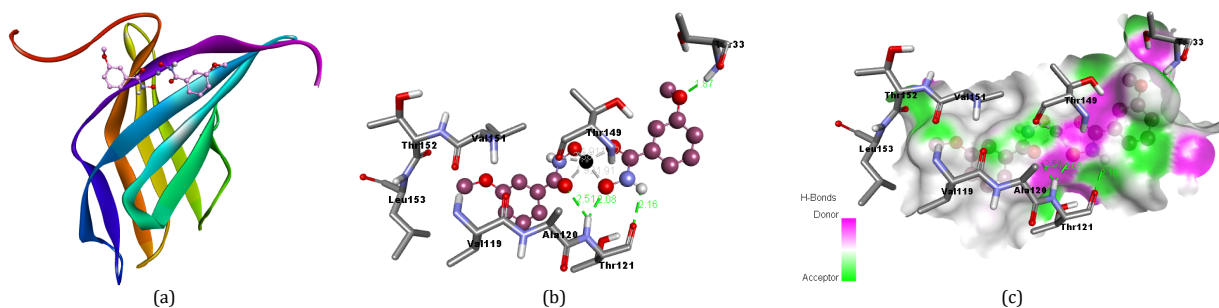
**Figure 3.** Interaction of complex with DNA (a) and sequence of residues around the complex (b).**Figure 4.** 2D interaction of the ligand with the protein.

The magnitude of the interaction between the receptor and the compounds can be assessed through the negative binding free energy. Both the ligand and the complex exhibited negative binding free energy, suggesting a favorable binding affinity with the protein. Keeping this in view, we report here the molecular docking studies of our ligand and its complex with *A. alternata* allergen alt 1 protein. The ligand, in its energy-minimized

docked conformation, adopted the lowest energy conformation within the protein groove, forming three hydrogen bonds (Figure 4 represents 2D interaction), i.e., the first hydrogen bond is observed between the hydrogen atom of the amino group of tyrosine A-55 residue of the protein and the methoxy oxygen of the ligand, with a specific bond length of 2.24 Å; second between the aspartic acid A-83 residue and hydroxamic

Table 7. Docking score of the ligand and complex with the 3VOR protein.

Thermodynamic parameters (Kcal/mol)	Ligand	Complex
Free energy of binding	-5.20	-8.25
Mean binding energy	-5.20	-8.25
Final intermolecular energy	-5.79	-9.45
Electrostatic energy	-0.43	-0.17
Vdw + H bond + desolve energy	-5.36	-9.27
Final total internal energy	-0.26	-0.53
Free energy (A)	-1368.76	-1371.13
Torsional free energy	+0.60	+1.19
Internal energy (U)	-4.53	-6.89
Unbound system energy	-0.26	-0.53
Inhibition constant (μM) (T = 298.15 K)	155.40	891.45
Entropy (S) (Kcal/mol/K)	4.58	4.58
Partition function (Q)	10.08	10.12
Type and number of binding formed	3 Hydrogen bonds (1.62, 1.96 and 2.24 Å)	4 Hydrogen bonds (1.87, 2.08, 2.16 and 2.51 Å)

**Figure 5.** (a) Docked pose of the ligand with protein; (b) interaction of amino acid residues; and (c) representation of the H-bonding surface.**Figure 6.** (a) Docked pose of the complex with protein; (b) interaction of amino acid residues; and (c) representation of the H-bonding surface.

oxygen (1.62 Å) and third between lysine A-80 and carbonyl oxygen (1.96 Å) through H- π interaction (Figure 5a-c) which affirms a docking score of -5.20 Kcal/mol. The corresponding zinc complex established four hydrogen bonds, *i.e.*, 2 H bond between one carbonyl and one hydroxamic oxygen of complex with H of Alanine-120 residue of the protein (2.08 and 2.51 Å); the third H bond between H present on nitrogen in hydroxamic group and Threonine-121 residue bond distances of 2.16 Å (Figure 6a-c). The fourth interaction was inferred between H of Threonine-33 residue and methoxy oxygen of the complex with a bond length of 1.87 Å. The complex was found to have a docking score of -8.25 kcal/mol as a result of H- π interaction. The complex formed a greater number of hydrogen bonds and attractive forces with various amino acid residues compared to those of the ligand, bolstering the findings of *in vitro* antimicrobial studies. This suggests that the complex has a higher binding affinity, indicating robust binding to the protein, as supported by its binding score. Consequently, the more negatively correlated binding free energies denote a stronger binding affinity, and the interactions between the target and the compounds are noncovalent in nature. Table 7 represents the various parameters obtained from the docking results of ligand and its Zn(II) complex, and Figures 4-6 represent the docked pose, their 3D interaction, and H bonding surface representation, respectively.

4. Conclusions

A biologically potent Zn(II) complex has been synthesized from potassium 3-methoxybenzohydroxamate, KHL. The complex has been characterized by physicochemical (elemental analysis) and spectral techniques (IR, ^1H NMR, ^{13}C NMR, and UV-visible). IR and ^{13}C NMR studies confirmed bonding through carbonyl and hydroxamic oxygens (O,O coordination). On the basis of analyses encompassing physicochemical characteristics, spectral data, and DFT investigations, it is proposed that zinc adopts a mononuclear four-coordinate structure with a distorted tetrahedral geometry. DFT investigations indicate that the complex exhibits enhanced stability and reduced reactivity compared to the ligand, characterized by a wider HOMO-LUMO band gap (ΔE).

The complex has shown promising antimicrobial activity against bacteria tested using the MIC method. It is highly effective against *E. coli* and *A. alternata*, with an MIC value of 7.80 $\mu\text{g/mL}$, comparable to the standard drugs tetracycline and amphotericin B. *In vitro* antimicrobial evaluation demonstrated that the synthesized complex exhibits greater potency compared to that of its unbound ligand, indicating its biological significance. Cytotoxicity investigations revealed an improved efficacy of the complex against L20B cell lines, demonstrating increased anticancer activity specific to cancer cell lines of

rhabdomyosarcoma. At a concentration of 35 µg/mL, the complex achieved a cell viability range of 3 to 1%, indicating superior cellular inhibition.

Assessing the efficacy of the synthesized complex hinges on its ability to interact with the binding interface linking the spike protein fragment and the receptor, thus illustrating its potential efficacy. To support biological efficacy, molecular docking was investigated to study interaction with the *Alternaria alternata* allergen Alt a1 (PDB ID: 3V0R). The findings revealed that the complex has a docking score of -8.25 kcal/mol, while the ligand revealed a docking score of -5.20 kcal/mol. The amino acid residues Tyr A-55, Asp A-83, ALA-120, Thr-121, and Thr-33 were mainly involved in the formation of hydrogen bonds. The results of molecular docking investigations reveal a higher binding energy for the complex compared to the ligand, indicating its proficiency in binding to the protein groove. Therefore, the biological studies affirmed the biological potential of the Zn(II) complex, which was supported by computational studies. Although numerous organic zinc derivatives exhibit potent biological activities, zinc-containing antimicrobial agents face challenges due to escalating bacterial resistance. Consequently, the pursuit of new zinc antimicrobials remains a formidable challenge. However, exploring this avenue holds significant promise, as the development of potent Zn(II) hydroxamates could yield promising antimicrobial candidates.

Acknowledgements

The authors express their gratitude to the Department of Chemistry of Himachal Pradesh University for providing laboratory facilities and UV-visible studies. The authors are also thankful to the Sophisticated Analytical Instrumentation Facility and the Central Instrumentation Laboratory at Panjab University, Chandigarh for recording FTIR, ¹H NMR, ¹³C NMR and elemental analysis. In addition, the authors thank the Central Potato Research Institute (CPRI) Shimla for providing fungal cultures. Lastly, the authors acknowledge the Department of Biotechnology at Himachal Pradesh University, Shimla, for providing laboratory facilities to carry out antimicrobial and cytotoxicity studies.

Disclosure statement

Conflict of interest: The authors declare that they have no conflict of interest. Ethical approval: All ethical guidelines have been adhered to. Sample availability: Samples of the compounds are available from the author.

CRedit authorship contribution statement

Conceptualization: Shubham Sharma, Meena Kumari; Methodology: Shubham Sharma, Meena Kumari; Software: Sohini Sharma; Validation: Shamsheer Singh Kanwar; Formal Analysis: Maridula Thakur; Investigation: Meena Kumari; Resources: Shamsheer Singh Kanwar; Data Curation: Shubham Sharma, Meena Kumari; Writing - Original Draft: Shubham Sharma; Writing - Review and Editing: Meena Kumari; Visualization: Shubham Sharma, Meena Kumari; Supervision: Meena Kumari.

ORCID and Email

Shubham Sharma

 shbhsharma360@gmail.com

 <https://orcid.org/0000-0003-2483-9524>


Maridula Thakur

 mriduthakur82@gmail.com

 <https://orcid.org/0000-0001-9788-5308>


Sohini Sharma

 sohinisharma920@gmail.com

 <https://orcid.org/0009-0008-0844-928X>

Shamsheer Singh Kanwar

 kanwarss2000@yahoo.com

 <https://orcid.org/0000-0002-3196-3366>

Meena Kumari

 drmeenakhandel@gmail.com

 <https://orcid.org/0000-0003-1107-3005>

References

- Eshghi, F.; Mehrabadi, Z.; Farsadrooh, M.; Hayati, P.; Javadian, H.; Karimi, M.; Karimi-Maleh, H.; Rostamnia, S.; Karaman, C.; Aghababaei, F. Photocatalytic degradation of remdesivir nucleotide pro-drug using [Cu(1-methylimidazole)₄(SCN)₂] nanocomplex synthesized by sonochemical process: Theoretical, hirshfeld surface analysis, degradation kinetic, and thermodynamic studies. *Environ. Res.* **2023**, *222*, 115321.
- Rashidi, N.; Soltanian Fard, M. J.; Hayati, P.; Janczak, J.; Yazdian, F. Green approach for fabrication of a novel Zn(II) supramolecular compound as new precursor to produce nano-sized Zinc(II) oxide: Crystallography, topology, Hirshfeld Surface Analysis and biological activities. *J. Mol. Struct.* **2020**, *1208*, 127885.
- Aghae, M.; Mohammadi, K.; Hayati, P.; Ahmadi, S.; Yazdian, F.; Gutierrez, A.; Rouhani, S.; Msagati, T. A. M. Morphology design and control of a novel 3D potassium metal-organic coordination polymer compound: Crystallography, DFT, thermal, and biological studies. *J. Mol. Struct.* **2021**, *1228*, 129434.
- Souri, B.; Reza Rezvani, A.; Abbasi, S.; Hayati, P.; Centore, R. An investigation on the morphology of a new coordination polymer via change effective factors based on eco-friendly sonochemical synthesis; new precursor for the preparation of cadmium(II) oxide. *Inorganica Chim. Acta* **2019**, *498*, 119134.
- Fard, M. J. S.; Hayati, P.; Naraghi, H. S.; Tabeie, S. A. Synthesis and characterization of a new nano lead(II) 0-D coordination supramolecular compound: A precursor to produce pure phase nano-sized lead(II) oxide. *Ultrason. Sonochem.* **2017**, *39*, 129–136.
- Abedi, M.; Mahmoudi, G.; Hayati, P.; Machura, B.; Zubkov, F. I.; Mohammadi, K.; Bahrami, S.; Derikvandi, H.; Mehrabadi, Z.; Kirillov, A. M. A 3D heterometallic Ni(ii)/K(i) MOF with a rare rna topology: synthesis, structural features, and photocatalytic dye degradation modeling. *New J Chem* **2019**, *43*, 17457–17465.
- Giachi, G.; Pallecchi, P.; Romualdi, A.; Ribechini, E.; Lucejko, J. J.; Colombini, M. P.; Mariotti Lippi, M. Ingredients of a 2,000-y-old medicine revealed by chemical, mineralogical, and botanical investigations. *Proc. Natl. Acad. Sci. U. S. A.* **2013**, *110*, 1193–1196.
- Interrelations between essential metal ions and human diseases*; Sigel, A.; Sigel, H.; Sigel, R. K. O., Eds.; Springer Netherlands: Dordrecht, 2013.
- Prasad, A. S. Zinc in human health: Effect of zinc on immune cells. *Mol. Med.* **2008**, *14*, 353–357.
- Broadley, M. R.; White, P. J.; Hammond, J. P.; Zelko, I.; Lux, A. Zinc in plants. *New Phytol.* **2007**, *173*, 677–702.
- Sugarman, B. Zinc and infection. *Clin. Infect. Dis.* **1983**, *5*, 137–147.
- Handbook of nutrition and food, second edition*; Berdanier, C. D.; Dwyer, J. T.; Feldman, E. B., Eds.; 2nd ed.; CRC Press: Boca Raton, FL, 2007.
- Hambidge, K. M.; Krebs, N. F. Zinc deficiency: A special Challenge1. *J. Nutr.* **2007**, *137*, 1101–1105.
- Agren, M. S.; Franzen, L.; Chvapil, M. Effects on wound healing of zinc oxide in a hydrocolloid dressing. *J. Am. Acad. Dermatol.* **1993**, *29*, 221–227.
- Lansdown, A. B. G. Influence of zinc oxide in the closure of open skin wounds. *Int. J. Cosmet. Sci.* **1993**, *15*, 83–85.
- Stromberg, H.-E.; Agren, M. S. Topical zinc oxide treatment improves arterial and venous leg ulcers. *Br. J. Dermatol.* **1984**, *111*, 461–468.
- Abendrot, M.; Chęcińska, L.; Kusz, J.; Lisowska, K.; Zawadzka, K.; Felczak, A.; Kalinowska-Lis, U. Zinc(II) complexes with amino acids for potential use in dermatology: Synthesis, crystal structures, and antibacterial activity. *Molecules* **2020**, *25*, 951.
- Raducka, A.; Świątkowski, M.; Korona-Głowniak, I.; Kaproń, B.; Plech, T.; Szczesio, M.; Gobis, K.; Szykowska-Jóźwik, M. I.; Czyłkowska, A. Zinc coordination compounds with benzimidazole derivatives: Synthesis, structure, antimicrobial activity and potential anticancer application. *Int. J. Mol. Sci.* **2022**, *23*, 6595.
- Hall, S. C.; Smith, D. R.; Dyavar, S. R.; Wyatt, T. A.; Samuelson, D. R.; Bailey, K. L.; Knoell, D. L. Critical role of Zinc transporter (ZIP8) in myeloid innate immune cell function and the host response against bacterial pneumonia. *J. Immunol.* **2021**, *207*, 1357–1370.
- Manieri, T. M.; Sensi, S. L.; Squitti, R.; Cerchiaro, G. Structural effects of stabilization and complexation of a zinc-deficient superoxide dismutase. *Heliyon* **2021**, *7*, e06100.
- Wąsowicz, W.; Kantorski, J.; Perek, D.; Popadiuk, S. Concentration of zinc and zinc-copper superoxide dismutase activity in red blood cells in normals and children with cancer. *Clin. Chem. Lab. Med.* **1989**, *27*, 413–418.
- Yashwantrao Patil, R.; More, H. N. Antioxidants with multivitamin and mineral supplementation attenuates chemotherapy or radiotherapy-induced oxidative stress in cancer patients. *Ind. J. Pharm. Educ.* **2020**, *54*, 484–490.
- Stefanidou, M.; Maravelias, C.; Dona, A.; Spiliopoulou, C. Zinc: a multipurpose trace element. *Arch. Toxicol.* **2006**, *80*, 1–9.
- Jansen, J.; Karges, W.; Rink, L. Zinc and diabetes — clinical links and molecular mechanisms. *J. Nutr. Biochem.* **2009**, *20*, 399–417.

- [25]. Emami, S.; Hosseini-mehr, S. J.; Taghdisi, S. M.; Akhlaghpour, S. Kojic acid and its manganese and zinc complexes as potential radioprotective agents. *Bioorg. Med. Chem. Lett.* **2007**, *17*, 45–48.
- [26]. Jiang, Z.; Shao, J.; Yang, T.; Wang, J.; Jia, L. Pharmaceutical development, composition and quantitative analysis of phthalocyanine as the photosensitizer for cancer photodynamic therapy. *J. Pharm. Biomed. Anal.* **2014**, *87*, 98–104.
- [27]. Nakayama, A.; Hiromura, M.; Adachi, Y.; Sakurai, H. Molecular mechanism of antidiabetic zinc–allixin complexes: regulations of glucose utilization and lipid metabolism. *J. Biol. Inorg. Chem.* **2008**, *13*, 675–684.
- [28]. Sakurai, H.; Yoshikawa, Y.; Yasui, H. Current state for the development of metallopharmaceutics and anti-diabetic metal complexes. *Chem. Soc. Rev.* **2008**, *37*, 2383–2392.
- [29]. d'Angelo, J.; Morgant, G.; Ghermani, N. E.; Desmaële, D.; Fraise, B.; Bonhomme, F.; Dichi, E.; Sghaier, M.; Li, Y.; Journaux, Y.; Sorenson, J. R. Crystal structures and physico-chemical properties of Zn(II) and Co(II) tetraaqua(3-nitro-4-hydroxybenzoato) complexes: Their anticonvulsant activities as well as related (5-nitrosalicylato)–metal complexes. *Polyhedron* **2008**, *27*, 537–546.
- [30]. Zhou, Q.; Hambley, T. W.; Kennedy, B. J.; Lay, P. A.; Turner, P.; Warwick, B.; Biffin, J. R.; Regtop, H. L. Syntheses and characterization of anti-inflammatory dinuclear and mononuclear zinc indomethacin complexes. Crystal structures of [Zn₂(indomethacin)₄(L)₂] (L = *N,N*-dimethylacetamide, pyridine, 1-methyl-2-pyrrolidinone) and [Zn(indomethacin)₂(L)₁]₂ (L₁ = ethanol, methanol). *Inorg. Chem.* **2000**, *39*, 3742–3748.
- [31]. Kasuga, N. C.; Sekino, K.; Ishikawa, M.; Honda, A.; Yokoyama, M.; Nakano, S.; Shimada, N.; Koumo, C.; Nomiya, K. Synthesis, structural characterization and antimicrobial activities of 12 zinc(II) complexes with four thiosemicarbazone and two semicarbazone ligands. *J. Inorg. Biochem.* **2003**, *96*, 298–310.
- [32]. Li, Z.-Q.; Wu, F.-J.; Gong, Y.; Hu, C.-W.; Zhang, Y.-H.; Gan, M.-Y. Synthesis, characterization and activity against *staphylococcus* of metal(II)-gatifloxacin complexes. *Chin. J. Chem.* **2007**, *25*, 1809–1814.
- [33]. Chen, Z.-F.; Xiong, R.-G.; Zhang, J.; Chen, X.-T.; Xue, Z.-L.; You, X.-Z. 2D molecular square grid with strong blue fluorescent emission: A complex of norfloxacin with zinc(II). *Inorg. Chem.* **2001**, *40*, 4075–4077.
- [34]. Yernale, N. G.; Udayagiri, M. D.; Mruthyunjayaswam, B. H. M. Synthesis, characterization, mass spectral fragmentation, thermal study and biological evaluation of new Schiff base ligand and its metal(II) complexes derived from 4-(diethylamino)salicylaldehyde and thiazole moiety. *Eur. J. Chem.* **2016**, *7*, 56–65.
- [35]. Dongare, G. M.; Aswar, A. S. A heterocyclic *N'*-(4-(diethylamino)-2-hydroxybenzylidene)-4-oxopiperidine-1-carbohydrazide Schiff base ligand and its metal complexes: Synthesis, structural characterization, thermal behavior, fluorescence properties, and biological activities. *Eur. J. Chem.* **2022**, *13*, 415–425.
- [36]. Seda, S. H.; Abdel Aziz, A. A. Synthesis, spectral characterization, antimicrobial, DNA binding and antioxidant studies of Co(II), Ni(II), Cu(II) and Zn(II) metal complexes of novel thiosalen analog N2S2. *Eur. J. Chem.* **2015**, *6*, 189–198.
- [37]. Shaikh, I.; Vohra, A.; Devkar, R.; Jadeja, R. Synthesis, characterization, structural features and cytotoxicity of innovative zinc(II) complex derived from ONS-donor thio-Schiff base of acyl pyrazolone. *Eur. J. Chem.* **2019**, *10*, 131–138.
- [38]. El-Henawy, A. A.; Hanafy, A. I. Synthesis, characterization, DNA-binding and biological activity of Zn(II) complexes of sulfadiazine with different amino acids. *Eur. J. Chem.* **2015**, *6*, 117–126.
- [39]. Tarushi, A.; Karafrou, Z.; Kljun, J.; Turel, I.; Psomas, G.; Papadopoulos, A. N.; Kessissoglou, D. P. Antioxidant capacity and DNA-interaction studies of zinc complexes with a non-steroidal anti-inflammatory drug, mefenamic acid. *J. Inorg. Biochem.* **2013**, *128*, 85–96.
- [40]. Kovala-Demertzi, D.; Yadav, P. N.; Wiecek, J.; Skoulika, S.; Varadinova, T.; Demertzi, M. A. Zinc(II) complexes derived from pyridine-2-carbaldehyde thiosemicarbazone and (1E)-1-pyridin-2-ylethan-1-one thiosemicarbazone. Synthesis, crystal structures and antiproliferative activity of zinc(II) complexes. *J. Inorg. Biochem.* **2006**, *100*, 1558–1567.
- [41]. Belicchi Ferrari, M.; Bisceglie, F.; Pelosi, G.; Tarasconi, P.; Albertini, R.; Pinelli, S. New methyl pyruvate thiosemicarbazones and their copper and zinc complexes: synthesis, characterization, X-ray structures and biological activity. *J. Inorg. Biochem.* **2001**, *87*, 137–147.
- [42]. Di Vaira, M.; Bazzicalupi, C.; Orioli, P.; Messori, L.; Bruni, B.; Zatta, P. Cloiquinol, a drug for Alzheimer's disease specifically interfering with brain metal metabolism: Structural characterization of its zinc(II) and copper(II) complexes. *Inorg. Chem.* **2004**, *43*, 3795–3797.
- [43]. Gupta, S. P. *Hydroxamic acids: A unique family of chemicals with multiple biological activities*; Springer Science & Business Media, 2013.
- [44]. Sow, I. S.; Gelbecke, M.; Dufraes, F.; Robeyns, K. Crystal structures of a series of hydroxamic acids. *Molbank* **2023**, *2023*, M1637.
- [45]. Fazary, A. E.; Khalil, M. M.; Fahmy, A.; Tantawy, A. The Role of Hydroxamic Acids in Biochemical Processes. *Med J Islamic World Acad Sci* **2001**, *14*, 109–116
- https://jag.journalagent.com/z4/download_fulltext.asp?pdid=ias&plng=eng&un=IAS-97759.
- [46]. Raymond, K. Biomimetic metal encapsulation. *Coord. Chem. Rev.* **1990**, *105*, 135–153.
- [47]. Sharma, N.; Kumari, M.; Kumar, V.; Chaudhry, S. C.; Kanwar, S. S. Synthesis, characterization, and antimicrobial activity of oxovanadium(IV)hydroxamate complexes. *J. Coord. Chem.* **2010**, *63*, 1940–1950.
- [48]. Farkas, E.; Enyedy, É. A.; Zékány, L.; Deák, G. Interaction between iron(II) and hydroxamic acids: oxidation of iron(II) to iron(III) by desferrioxamine B under anaerobic conditions. *J. Inorg. Biochem.* **2001**, *83*, 107–114.
- [49]. Alagta, A.; Felhósi, I.; Kálmán, E. Hydroxamic acid corrosion inhibitor for steel in aqueous solution. *Mater. Sci. For.* **2007**, *537–538*, 81–88.
- [50]. Codd, R. Traversing the coordination chemistry and chemical biology of hydroxamic acids. *Coord. Chem. Rev.* **2008**, *252*, 1387–1408.
- [51]. Benini, S.; Rypniewski, W. R.; Wilson, K. S.; Miletti, S.; Ciurli, S.; Mangani, S. The complex of *Bacillus pasteurii* urease with acetohydroxamate anion from X-ray data at 1.55 Å resolution. *J. Biol. Inorg. Chem.* **2000**, *5*, 110–118.
- [52]. Scolnick, L. R.; Clements, A. M.; Liao, J.; Crenshaw, L.; Hellberg, M.; May, J.; Dean, T. R.; Christianson, D. W. Novel binding mode of hydroxamate inhibitors to human carbonic anhydrase II. *J. Am. Chem. Soc.* **1997**, *119*, 850–851.
- [53]. Kumar, A.; Priya, B.; Thakur, A.; Sharma, N. *in vitro* cytotoxicity and DNA binding studies of newly synthesized oxidovanadium (IV) complexes of Nitro-substituted benzohydroxamate ligands as prospective vanadodrug compounds. *Adv. Sci. Eng. Med.* **2018**, *10*, 27–37.
- [54]. Choudhary, V. K.; Bhatt, A. K.; Sharma, N. Theoretical and spectroscopic evidence on a new triphenyltin(IV) 3,5-dinitrosalicylhydroxamate complex: synthesis, structural characterization, and biological screening. *J. Coord. Chem.* **2020**, *73*, 947–968.
- [55]. Sharma, S.; Sharma, N.; Kumari, M.; Thakur, M. Synthesis, characterization and evaluation of antimicrobial potential of zinc(II) complexes of nitro-substituted hydroxamic acid chelators. *J. Coord. Chem.* **2022**, *75*, 1289–1302.
- [56]. Farkas, E.; Enyedy, É. A.; Csóka, H. A comparison between the chelating properties of some dihydroxamic acids, desferrioxamine B and acetohydroxamic acid. *Polyhedron* **1999**, *18*, 2391–2398.
- [57]. Syed, Z.; Sonu, K.; Dongre, A.; Sharma, G.; Sogani, M. A review on Hydroxamic Acids: Widespectrum Chemotherapeutic Agents. *Int. J. Biol. Biomed. Eng.* **2020**, *14*, 75–88.
- [58]. Vogel, A. I.; Jeffery, G. H. *Vogel's textbook of quantitative chemical analysis*; Longman Scientific and Technical, 1989.
- [59]. Neese, F.; Wennmohs, F.; Becker, U.; Riplinger, C. The ORCA quantum chemistry program package. *J. Chem. Phys.* **2020**, *152*, 224108.
- [60]. Zhurko, G. A.; Zhurko, D. A. Chemcraft - Graphical program for visualization of quantum chemistry computations. <http://www.chemcraftprog.com> (accessed Jan 5, 2024).
- [61]. Pettersen, E. F.; Goddard, T. D.; Huang, C. C.; Couch, G. S.; Greenblatt, D. M.; Meng, E. C.; Ferrin, T. E. UCSF Chimera—A visualization system for exploratory research and analysis. *J. Comput. Chem.* **2004**, *25*, 1605–1612.
- [62]. Morris, G. M.; Huey, R.; Lindstrom, W.; Sanner, M. F.; Belew, R. K.; Goodsell, D. S.; Olson, A. J. AutoDock4 and AutoDockTools4: Automated docking with selective receptor flexibility. *J. Comput. Chem.* **2009**, *30*, 2785–2791.
- [63]. Biovia, D. S.; Berman, H. M.; Westbrook, J.; Feng, Z.; Gilliland, G.; Bhat, T. N.; Richmond, T. J., 2000. Dassault systemes BIOVIA, Discovery studio visualizer, v. 17.2, San Diego: Dassault Systemes, 2016.
- [64]. Hauser, C. R.; Renfrow Jr., W. B. Benzohydroxamic acid. *Organic Synth.* Coll. Vol. 2. A.H. Blatt (Ed.), John Wiley and Sons, New York. 1939, 19, 15.
- [65]. Choudhary, V. K.; Kumar, A.; Sharma, N. Potential bioactive mononuclear diorganotin(IV) phenoxyacetohydroxamate complexes: synthesis, characterization and antimicrobial evaluation. *Main Group Met. Chem.* **2018**, *41* (1,2), 27–32 <https://doi.org/10.1515/mgmc-2017-0056>.
- [66]. Becke, A.D. Density-Functional Thermochemistry. III. The Role of Exact Exchange. *J. Chem. Phys.* **1993**, *98*, 5648–5652.
- [67]. Schäfer, A.; Horn, H.; Ahlrichs, R. Fully optimized contracted Gaussian basis sets for atoms Li to Kr. *J. Chem. Phys.* **1992**, *97*, 2571–2577.
- [68]. Determination of minimum inhibitory concentrations (MICs) of antibacterial agents by broth dilution. *Clin. Microbiol. Infect.* **2003**, *9*, ix–xv <https://doi.org/10.1046/j.1469-0691.2003.00790.x>.
- [69]. Sarker, S. D.; Nahar, L.; Kumarasamy, Y. Microtitre plate-based antibacterial assay incorporating resazurin as an indicator of cell growth, and its application in the *in vitro* antibacterial screening of phytochemicals. *Methods* **2007**, *42*, 321–324.
- [70]. Wayne, P.A. Clinical and Laboratory Standards Institute. Methods for Dilution Antimicrobial Susceptibility Tests for Bacteria that Grow Aerobically; Approved Standard In: CLSI Document M07-A9 (9th ed). Clinical and Laboratory Standards Institute; 2012.

- [71]. Rashidi, N.; Fard, M. J. S.; Hayati, P.; Janczak, J.; Yazdian, F.; Rouhani, S.; Msagati, T. A. M. Antibacterial and cytotoxicity assay of two new Zn(II) complexes: Synthesis, characterization, X-Ray structure, topology, Hirshfeld surface and thermal analysis. *J. Mol. Struct.* **2021**, *1231*, 129947.
- [72]. Hinson, A. R. P.; Jones, R.; Crose, L. E. S.; Belyea, B. C.; Barr, F. G.; Linardic, C. M. Human rhabdomyosarcoma cell lines for rhabdomyosarcoma research: Utility and pitfalls. *Front. Oncol.* **2013**, *3*, 183.
- [73]. Chruszcz, M.; Chapman, M. D.; Osinski, T.; Solberg, R.; Demas, M.; Porebski, P. J.; Majorek, K. A.; Pomés, A.; Minor, W. Alternaria alternata allergen Alt a 1: A unique β -barrel protein dimer found exclusively in fungi. *J. Allergy Clin. Immunol.* **2012**, *130*, 241-247.e9.
- [74]. Schrödinger, L.; DeLano, W. PyMOL, 2020, <http://www.pymol.org/pymol>.
- [75]. Mohapatra, R. K.; El-ajaily, M. M.; Alassbaly, F. S.; Sarangi, A. K.; Das, D.; Maihub, A. A.; Ben-Gweirif, S. F.; Mahal, A.; Suleiman, M.; Perekhoda, L.; Azam, M.; Al-Noor, T. H. DFT, anticancer, antioxidant and molecular docking investigations of some ternary Ni(II) complexes with 2-[(E)-[4-(dimethylamino)phenyl]methyleneamino]phenol. *Chem. Pap.* **2021**, *75*, 1005-1019.
- [76]. Geary, W. J. The use of conductivity measurements in organic solvents for the characterisation of coordination compounds. *Coord. Chem. Rev.* **1971**, *7*, 81-122.
- [77]. AbouEl-Enein, S. A.; El-Saied, F. A.; Kasher, T. I.; El-Wardany, A. H. Synthesis and characterization of iron(III), manganese(II), cobalt(II), nickel(II), copper(II) and zinc(II) complexes of salicylidene-N-anilinoacetohydrazone (H2L1) and 2-hydroxy-1-naphthylidene-N-anilinoacetohydrazone (H2L2). *Spectrochim. Acta A Mol. Biomol. Spectrosc.* **2007**, *67*, 737-743.
- [78]. Matijevic-Sosa, J.; Vinkovic, M.; Vikić-Topić, D. NMR spectroscopy of 2-hydroxy-1-naphthylidene Schiff bases with chloro and hydroxy substituted aniline moiety. **2006**, *79* (3), 489-495 <https://hrcak.srce.hr/5662>.
- [79]. Kohn, W.; Becke, A. D.; Parr, R. G. Density functional theory of electronic structure. *J. Phys. Chem.* **1996**, *100*, 12974-12980.
- [80]. Abdel-Latif, S. A.; Mohamed, A. A. Synthesis, spectroscopic characterization, first order nonlinear optical properties and DFT calculations of novel Mn(II), Co(II), Ni(II), Cu(II) and Zn(II) complexes with 1,3-diphenyl-4-phenylazo-5-pyrazolone ligand. *J. Mol. Struct.* **2018**, *1153*, 248-261.
- [81]. Chandrasekar, T.; Arunadevi, A.; Raman, N. Synthesis, spectral characterization, DNA-binding and antimicrobial profile of biological active mixed ligand Schiff base metal(II) complexes incorporating 1,8-diaminonaphthalene. *J. Coord. Chem.* **2021**, *74*, 804-822.
- [82]. Zia-ur-Rehman; Muhammad, N.; Shuja, S.; Ali, S.; Butler, I. S.; Meetsma, A.; Khan, M. New dimeric, trimeric and supramolecular organotin(IV) dithiocarboxylates: Synthesis, structural characterization and biocidal activities. *Polyhedron* **2009**, *28*, 3439-3448.
- [83]. Sultan, J. S.; Lateef, S. M.; Rashid, D. K. Synthesis, characterization and antibacterial activity of mixed ligand (HL) complexes Mn(II), Co(II), Ni(II), Zn(II), Cd(II) and Hg(II) with azide (N₃⁻). *Open J. Inorg. Chem.* **2015**, *05*, 102-111.
- [84]. Shujah, S.; Zia-ur-Rehman; Muhammad, N.; Shah, A.; Ali, S.; Meetsma, A.; Hussain, Z. Homobimetallic organotin(IV) complexes with hexadentate Schiff base: Synthesis, crystal structure and antimicrobial studies. *J. Organomet. Chem.* **2014**, *759*, 19-26.
- [85]. Sahraei, A.; Kargar, H.; Hakimi, M.; Tahir, M. N. Synthesis, characterization, crystal structures and biological activities of eight-coordinate zirconium(IV) Schiff base complexes. *Transit. Met. Chem.* **2017**, *42*, 483-489.
- [86]. Eslami Moghadam, M.; Hasanzadeh Esfahani, M.; Behzad, M.; Zolghadri, S.; Ramezani, N.; Azadi, Y. New platinum (II) complexes based on schiff bases: synthesis, specification, X-ray structure, ADMET, DFT, molecular docking, and anticancer activity against breast cancer. *J. Biol. Inorg. Chem.* **2023**, *28*, 519-529.



Copyright © 2024 by Authors. This work is published and licensed by Atlanta Publishing House LLC, Atlanta, GA, USA. The full terms of this license are available at <https://www.eurjchem.com/index.php/eurjchem/terms> and incorporate the Creative Commons Attribution-Non Commercial (CC BY NC) (International, v4.0) License (<http://creativecommons.org/licenses/by-nc/4.0>). By accessing the work, you hereby accept the Terms. This is an open access article distributed under the terms and conditions of the CC BY NC License, which permits unrestricted non-commercial use, distribution, and reproduction in any medium, provided the original work is properly cited without any further permission from Atlanta Publishing House LLC (European Journal of Chemistry). No use, distribution, or reproduction is permitted which does not comply with these terms. Permissions for commercial use of this work beyond the scope of the License (<https://www.eurjchem.com/index.php/eurjchem/terms>) are administered by Atlanta Publishing House LLC (European Journal of Chemistry).